Accessing Phonon Polaritons in Hyperbolic Crystals by Angle-Resolved Photoemission Spectroscopy

Andrea Tomadin,[1] Alessandro Principi,[2] Justin C. W. Song,[3] Leonid S. Levitov,[4,*] and Marco Polini[5,1,†]
[1]NEST, Istituto Nanoscienze-CNR and Scuola Normale Superiore, I-56126 Pisa, Italy
[2]Department of Physics and Astronomy, University of Missouri, Columbia, Missouri 65211, USA
[3]Walter Burke Institute for Theoretical Physics and Institute for Quantum Information and Matter, California Institute of Technology, Pasadena, California 91125, USA
[4]Department of Physics, Massachusetts Institute of Technology, Cambridge, Massachusetts 02139, USA
[5]Istituto Italiano di Tecnologia, Graphene Labs, Via Morego 30, I-16163 Genova, Italy
(Received 22 April 2015; published 21 August 2015)

Recently studied hyperbolic materials host unique phonon-polariton (PP) modes. The ultrashort wavelengths of these modes, as well as their low damping, hold promise for extreme subdiffraction nanophotonics schemes. Polar hyperbolic materials such as hexagonal boron nitride can be used to realize long-range coupling between PP modes and extraneous charge degrees of freedom. The latter, in turn, can be used to control and probe PP modes. Here we analyze coupling between PP modes and plasmons in an adjacent graphene sheet, which opens the door to accessing PP modes by angle-resolved photoemission spectroscopy (ARPES). A rich structure in the graphene ARPES spectrum due to PP modes is predicted, providing a new probe of PP modes and their coupling to graphene plasmons.

DOI: 10.1103/PhysRevLett.115.087401 PACS numbers: 78.67.Wj, 73.20.Mf, 81.05.Xj

Introduction.—The intrinsic hyperbolic character [1] of hexagonal boron nitride (hBN) grants a unique platform for realizing deep-subwavelength nanophotonic schemes. Key to these developments are phonon-polariton (PP) modes that exist within *reststrahlen* frequency bands [2,3], characterized by wavelengths that can be as small as 1–100 nm. Highly directional, these modes exhibit deep subdiffraction confinement of light with wavelengths far shorter than those of exciton-polaritons in semiconductor microcavities [4]. PPs have been shown to propagate with low losses [2,3] besting artificial metallic-resonator metamaterial schemes, and holding promise for transformation optics applications [5,6].

Harnessing PP modes depends on gaining access to their response over a wide wave number and energy bandwidths. However, to date these modes have only been studied within a small frequency range limited by laser choice (e.g., $170\ \text{meV} \lesssim \hbar\omega \lesssim 200\ \text{meV}$ via the scattering-type near-field optical spectroscopy technique [2]), or at specific wavelengths fixed by the sample geometry [3]. New approaches allowing researchers to resolve the PP modes at short wavelengths and over a broad range of energies are therefore highly desirable.

Here we describe an angle-resolved photoemission spectroscopy (ARPES) [7] scheme to achieve broadband energy-resolved access to ultrashort wavelength PPs in hBN. At first glance, ARPES access to PPs in a wide-band-gap insulator (hBN) where no free carriers are available may seem counterintuitive. To circumvent this difficulty, we employ coupling to charge degrees of freedom in graphene monolayer placed atop a hBN slab. Strong coupling [8–13] between hBN Fabry-Pérot PP modes and the collective charge oscillations in a doped graphene sheet [14] gives rise to hybrid excitations—plasmon-phonon polaritons—which from now on we will refer to as hybrid plasmons. This opens up new channels for quasiparticle decay yielding a rich structure of dispersive satellite features in the graphene ARPES spectrum, marked by red arrows in Fig. 1. The Fabry-Pérot resonances and the associated structure in ARPES spectrum are tunable by hBN slab thickness.

As discussed below, a one-atom-thick conducting material like graphene, placed atop an insulating hyperbolic crystal, fully enables ARPES studies of PP modes. The advantage of this approach is that ARPES achieves extreme resolution over a wide range of wave vectors $\boldsymbol{k}$ (from the corners K, K' of the graphene Brillouin zone to the Fermi wave number k_F in graphene) and energies $\hbar\omega$, with all energies below the Fermi energy being probed simultaneously. This gives an additional benefit, besides tunability, in that the entire range of frequencies and wave numbers can be covered within a single experiment.

From a more fundamental perspective, ARPES will also be an ideal tool to investigate whether effective electron-electron (e-e) interactions mediated by the exchange of PPs are capable of driving electronic systems towards correlated states. We also note that the tunable coupling between graphene quasiparticles and the complex excitations of its supporting substrate can be used to achieve control over the *spectral* properties of graphene carriers, including their decay rates, renormalized velocities, etc.

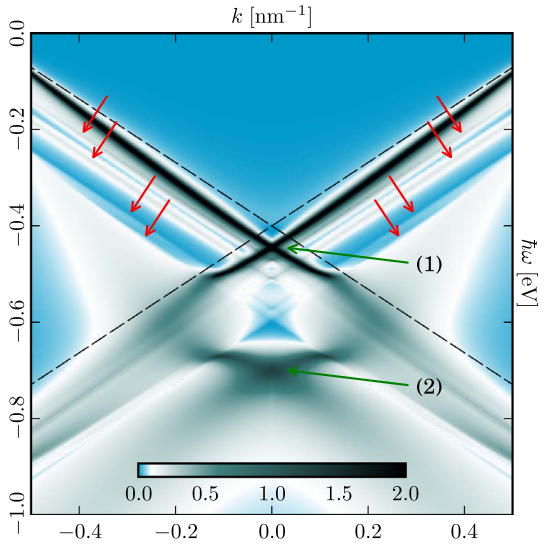

FIG. 1 (color online). Signatures of PP modes in the quasiparticle spectral function $\mathcal{A}(\boldsymbol{k},\omega)$ of a doped graphene sheet placed over a hBN slab, obtained from Eqs. (3) and (6). The Fermi energy is positioned at $\omega = 0$. The black linearly dispersing quasiparticle bands display a clear Dirac crossing labeled by (1). The broad spectral feature labeled by (2) is plasmaron excitation related to the emission of the hybrid plasmon mode with highest energy, see Eqs. (4), (5) and accompanying discussion. Its energy is derived from the highest plasmon resonance, labeled by the uppermost green dot in Fig. 2(a). Emission of Fabry-Pérot PP modes [see Fig. 2(a)] gives rise to four dispersive satellite bands running parallel to the main quasiparticle bands (marked by red arrows). The feature (2) is mainly plasmonic, whereas the satellite bands are mostly due to PP modes. Parameters used: Fermi energy $\varepsilon_F = 400$ meV, hBN slab thickness $d = 60$ nm, $\epsilon_a = 1$ (vacuum), $\epsilon_b = 3.9$ (SiO_2). The color bar refers to the values of $\hbar\mathcal{A}(\boldsymbol{k},\omega)$ in eV.

Phonon-polaritons and hybrid plasmons.—We consider a vertical heterostructure—see inset in Fig. 2(b)—comprised of a graphene sheet located at $z = 0$, placed atop an anisotropic insulator of thickness d with dielectric tensor $\hat{\boldsymbol{\epsilon}} = \mathrm{diag}(\epsilon_x, \epsilon_y, \epsilon_z)$. The two half-spaces $z > 0$ and $z < -d$ are treated as homogeneous isotropic media with dielectric constants ϵ_a and ϵ_b. For a *uniaxial* ($\epsilon_y = \epsilon_x$) dielectric, the Fourier transform of the Coulomb interaction potential in the graphene plane is given by

$$V_{\boldsymbol{q},\omega} = v_q \frac{\sqrt{\epsilon_x\epsilon_z} + \epsilon_b \tanh(qd\sqrt{\epsilon_x/\epsilon_z})}{\sqrt{\epsilon_x\epsilon_z} + \tilde{\epsilon}\tanh(qd\sqrt{\epsilon_x/\epsilon_z})}, \qquad (1)$$

where $v_q = 4\pi e^2/q(\epsilon_a + \epsilon_b)$ and $\tilde{\epsilon} = (\epsilon_x\epsilon_z + \epsilon_a\epsilon_b)/(\epsilon_a + \epsilon_b)$. A more general result, which is valid in the case $\epsilon_y \neq \epsilon_x$, can also be derived [15]. In the case of hBN, the components ϵ_x and ϵ_z of the dielectric tensor have resonant dependence on frequency ω in the midinfrared [18]. Here we use a simple parametrization for $\epsilon_{x,z}(\omega)$ [15]; a more realistic parametrization can be found in the Supplemental Material of Ref. [11].

Standing PP modes [2] correspond to poles of the interaction in Eq. (1) *inside* the reststrahlen bands. Changing tanh to tan in Eq. (1) we obtain Fabry-Pérot PP modes which from now on will be referred to simply as PP modes. Illustrative numerical results for $d = 10$ and $d = 60$ nm and analytical expressions, which are valid for $qd \ll 1$ and $qd \gg 1$, can be found in [15].

The coupling of PP modes in a hBN slab to plasmons in a nearby graphene sheet is well captured by the random phase approximation (RPA) [19]. In the RPA the interacting electron system is taken to respond as an ideal Fermi gas to the Hartree potential determined by the external charges and by the polarization charges, while local field effects due to exchange and correlations are neglected [19]. This gives

$$W_{\boldsymbol{q},\omega} = \frac{V_{\boldsymbol{q},\omega}}{\varepsilon(\boldsymbol{q},\omega)} \equiv \frac{V_{\boldsymbol{q},\omega}}{1 - V_{\boldsymbol{q},\omega}\chi_0(q,\omega)}. \qquad (2)$$

Here $\varepsilon(\boldsymbol{q},\omega)$ is the RPA dielectric function and $\chi_0(q,\omega)$ is the density-density response function of a 2D massless Dirac fermion fluid [20]. In addition to the poles of $V_{\boldsymbol{q},\omega}$ which describe the slab PP modes, new poles of $W_{\boldsymbol{q},\omega}$ emerge, given by weakly damped solutions $\omega = \Omega_{\boldsymbol{q}} - i0$ of the equation $\varepsilon(\boldsymbol{q},\omega) = 0$.

Interestingly, out of many PP modes only a few are strongly hybridized with plasmons. Illustrative numerical results for $\varepsilon_F = 400$ meV and $d = 60$ nm are shown in Fig. 2(a). Solid lines represent the hybrid modes originating from graphene plasmons (dashed line) and standing PP modes in the hBN slab. Three strongly hybridized modes are marked by red lines; the majority of PP modes, however, remain essentially unhybridized with plasmons (such modes are marked by black lines). We also see that there are special q values (green circles) where group velocity equals v_F, a feature that will be crucial for our analysis below. The corresponding modes couple strongly to quasiparticles in graphene, as we now proceed to demonstrate.

Quasiparticle decay rates.—An excited quasiparticle with momentum $\boldsymbol{k}$ and energy $\hbar\omega$, created in graphene in an ARPES experiment [21–25], can decay through scattering processes involving electron-hole pairs or collective modes. The decay rate $\hbar/\tau_\lambda(\boldsymbol{k},\omega)$ for these processes can be calculated [19] from the imaginary part of the retarded quasiparticle self-energy $\Sigma_\lambda(\boldsymbol{k},\omega)$, i.e. $\hbar/\tau_\lambda(\boldsymbol{k},\omega) = -2\mathrm{Im}[\Sigma_\lambda(\boldsymbol{k},\omega)]$. In the RPA and at zero temperature we have [26,27]

$$\mathrm{Im}[\Sigma_\lambda(\boldsymbol{k},\omega)] = \sum_{\lambda'}\int \frac{d^2\boldsymbol{q}}{(2\pi)^2}\mathrm{Im}[W_{\boldsymbol{q},\omega-\xi_{\lambda',\boldsymbol{k}+\boldsymbol{q}}}]\mathcal{F}_{\lambda\lambda'} \times [\Theta(\hbar\omega - \xi_{\lambda',\boldsymbol{k}+\boldsymbol{q}}) - \Theta(-\xi_{\lambda',\boldsymbol{k}+\boldsymbol{q}})]. \qquad (3)$$

Here, $\mathcal{F}_{\lambda\lambda'} \equiv [1 + \lambda\lambda'\cos(\theta_{\boldsymbol{k},\boldsymbol{k}+\boldsymbol{q}})]/2$ is the chirality factor [26,27], $\xi_{\lambda,\boldsymbol{k}} = \lambda\hbar v_F k - \varepsilon_F$ is the Dirac band energy measured from the Fermi energy ε_F ($\lambda, \lambda' = \pm 1$), and

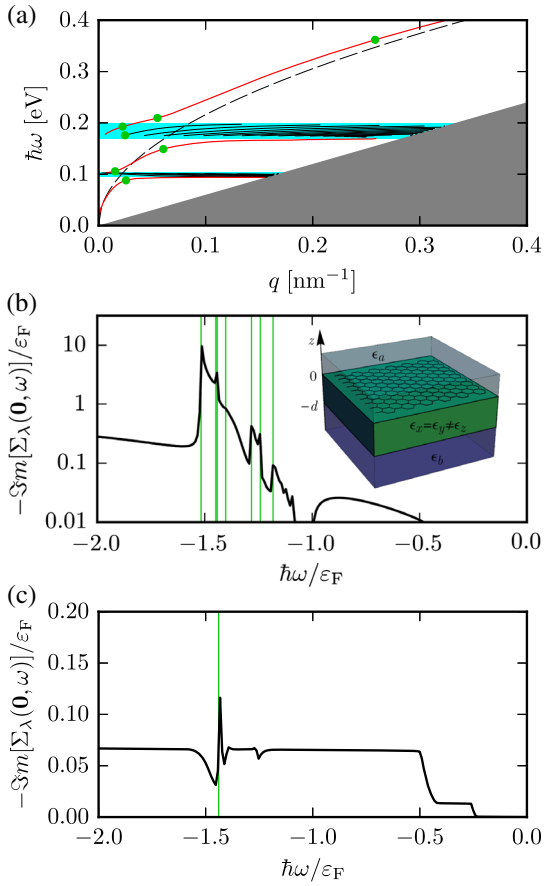

FIG. 2 (color online). (a) Dispersion relation $\Omega_{\boldsymbol{q}}$ of hybrid plasmon modes (solid lines) with parameters as in Fig. 1. The dashed line represents a Dirac plasmon [14]. Horizontal cyan areas denote the hBN reststrahlen bands. The gray-shaded area represents the intraband particle-hole continuum in graphene. Green dots mark the points where the hybrid plasmon group velocity equals v_F. (b) The quantity $-\mathrm{Im}[\Sigma_\lambda(\boldsymbol{k},\omega)]$ (in units of ε_F and evaluated at $\boldsymbol{k}=0$) is shown as a function of the rescaled frequency $\hbar\omega/\varepsilon_F$. Green vertical lines denote the values of $\hbar\omega/\varepsilon_F$ at which a hybrid plasmon peak is expected. The inset shows the vertical heterostructure analyzed in this work. (c) Same as in (b) but in the absence of e-e dynamical screening; obtained by replacing $W_{\boldsymbol{q},\omega} \to V_{\boldsymbol{q},\omega}$ in Eq. (3). Note a polaronic peak at $\hbar\omega \approx -1.42\varepsilon_F$. Results for other values of ε_F and d can be found in [15].

$\Theta(x)$ is the Heaviside step function. The quantity $\hbar\omega$ is also measured from the Fermi energy; $\theta_{\boldsymbol{k},\boldsymbol{k}+\boldsymbol{q}}$ is the angle between $\boldsymbol{k}$ and $\boldsymbol{k}+\boldsymbol{q}$. Equation (3) reduces to the standard Fermi golden rule result at order $\mathcal{O}(V^2_{\boldsymbol{q},\omega})$. Physically, it describes the decay rate for a process in which an initial state with momentum $\boldsymbol{k}$ and energy $\hbar\omega$ (measured from ε_F) decays into a final state with momentum $\boldsymbol{k}+\boldsymbol{q}$ and energy $\xi_{\lambda',\boldsymbol{k}+\boldsymbol{q}}$ (measured from ε_F). For $\omega<0$, the self-energy expresses the decay of *holes* created inside the Fermi sea. Fermi statistics requires the final state to be *occupied* so both band indices $\lambda'=\pm1$ are allowed in the case $\varepsilon_F>0$ that we consider here. Since ARPES measures the properties of holes produced in the Fermi sea by photoejection, only $\omega<0$ is relevant for this experimental probe in an n-doped graphene sheet.

To gain more insight into the behavior of $\mathrm{Im}[\Sigma_\lambda(\boldsymbol{k},\omega)]$ we focus on the initial hole states with momentum $\boldsymbol{k}=0$. In this case, the 2D integral in Eq. (3) reduces to a simple 1D quadrature. The initial hole energy is $E_i=\hbar\omega+\varepsilon_F$. The final hole energy is $E_f=\xi_{\lambda',\boldsymbol{q}}+\varepsilon_F=\lambda'\hbar v_F q$. When the difference $\Delta_{\lambda',q}\equiv E_f-E_i$ is equal to the real part of the mode energy $\hbar\Omega_{\boldsymbol{q}}$, the initial hole, which has been left behind after the photoejection of an electron, can decay by emitting a hybrid plasmon excitation. Since $\hbar\Omega_{\boldsymbol{q}}>\hbar v_F q$, but $\Delta_{\lambda',q}\le\hbar v_F q$ for intraband transitions, an initial hole state with $E_i<0$ can decay only into a final hole state with $E_f>0$. In particular, when the hybrid plasmon group velocity equals $\pm v_F$, namely

$$d\Omega_{\boldsymbol{q}}/dq=\hbar^{-1}d\Delta_{\lambda',q}/dq=\lambda' v_F, \tag{4}$$

such decay process is *resonant*. When these conditions are met, the interband contribution to $\mathrm{Im}[\Sigma_\lambda(0,\omega)]$ peaks at a characteristic value of ω and $\mathrm{Re}[\Sigma_\lambda(0,\omega)]$ changes sign rapidly around that frequency. This is nothing but a plasmaron excitation [28]. Within RPA, plasmaron is a quasiparticle comprising a hole moving with the same speed as plasmons. This is described by a solution of the Dyson equation, distinct from the ordinary quasiparticle pole of the one-body Green's function as $k\to k_F$ and $\omega\to0$.

The quantity $\mathrm{Im}[\Sigma_\lambda(0,\omega)]$ is plotted as a function of ω in Fig. 2(b), for $\varepsilon_F=400$ meV and $d=60$ nm. (The dependence on ε_F and d is discussed in [15].) We note several peaks in $\mathrm{Im}[\Sigma_\lambda(0,\omega)]$ for $\hbar\omega<-\varepsilon_F$ ($E_i<0$), which occur at values of $\hbar\omega$ that are in a one-to-one correspondence with the "resonant" frequency values such that the group velocity equals v_F, as shown in Fig. 2(a). Indeed, as stated above, peaks in $\mathrm{Im}[\Sigma_\lambda(0,\omega)]$ are expected at values of $\hbar\omega$—marked by green vertical lines in Fig. 2(b)—given by

$$\hbar\omega=\hbar v_F q^\star-\varepsilon_F-\hbar\Omega_{q^\star} \tag{5}$$

where $q^\star$ is the wave number at which the resonance condition in Eq. (4) is met. For example, the resonant mode at highest energy in Fig. 2(a), which occurs at $q^\star\approx0.26$ nm^{-1} and energy $\hbar\Omega_{q^\star}\approx0.36$ eV, yields a peak in $\mathrm{Im}[\Sigma_\lambda(0,\omega)]$ at $\hbar\omega/\varepsilon_F\approx-1.5$; see Fig. 2(b).

The dynamical screening due to e-e interactions is crucial for producing hybridized plasmons and resonances in Fig. 2(b). In contrast, for $\varepsilon(\boldsymbol{k},\omega)=1$, the off-shell decay rate $\mathrm{Im}[\Sigma_\lambda(0,\omega)]$ shows only a polaronic peak, due to the emission of a Fabry-Perót PP mode with group velocity equal to v_F; see Fig. 1 in Ref. [15].

The features in the ARPES spectral function, described at $k=0$ as outlined above, feature a characteristic k dependence. In particular, plasmaron resonance splits into a doublet dispersing with k and giving rise to a blurred X-shaped feature in Fig. 1. In this case, splitting and

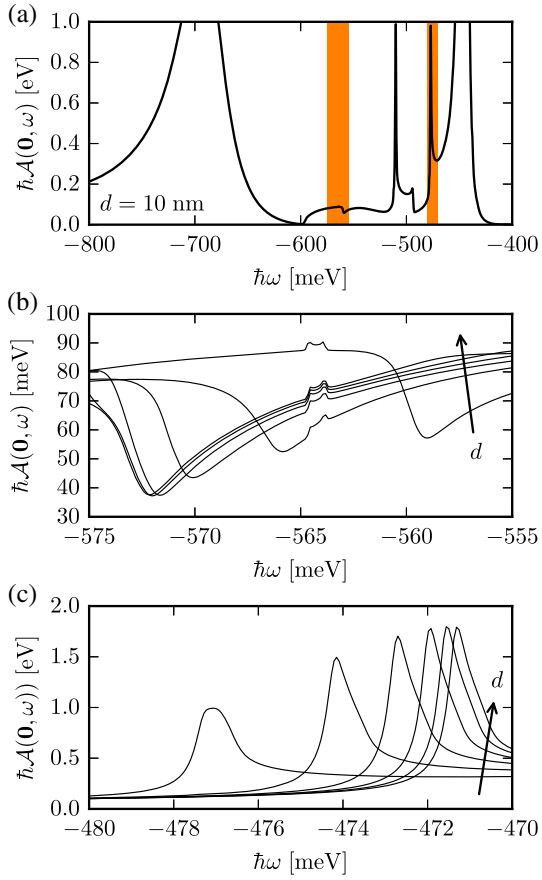

FIG. 3 (color online). (a) The quasiparticle spectral function $\mathcal{A}(\boldsymbol{k},\omega)$, evaluated at $|\boldsymbol{k}| = 10^{-3}k_F$, for $d = 10$ nm. The other parameters are as in Fig. 1. (b) and (c) Dependence on the hBN slab thickness d of the spectral function features highlighted in orange in (a). Different curves correspond to values of d on a uniform mesh from $d = 10$ to $d = 60$ nm.

dispersion can be understood by noting that at small k the relevant k and q are nearly parallel for the conduction-band states and nearly anti-parallel for the valence-band states. The features of the spectral function originating from PP modes (marked by red arrows in Fig. 1) show an approximately linear dispersion which closely tracks the edges of the Dirac continuum. This is so because of a relatively weak dispersion of PP modes and because of the off-shell character of the plasmons which mediate coupling between graphene electrons and the PP modes.

Quasiparticle spectral function.—An ARPES experiment [7] probes the quasiparticle spectral function $\mathcal{A}(\boldsymbol{k},\omega) = -\pi^{-1}\sum_\lambda \mathrm{Im}[G_\lambda(\boldsymbol{k},\omega)] = \sum_{\lambda=\pm1}\mathcal{A}_\lambda(\boldsymbol{k},\omega)$. Here, $G_\lambda(\boldsymbol{k},\omega)$ is the one-body Green's function in the band representation and

$$\mathcal{A}_\lambda(k,\omega) = -\frac{1}{\pi}\frac{\mathrm{Im}\Sigma_\lambda}{(\omega - \xi_{\lambda,\boldsymbol{k}}/\hbar - \mathrm{Re}\Sigma_\lambda/\hbar)^2 + (\mathrm{Im}\Sigma_\lambda/\hbar)^2}. \tag{6}$$

The real part $\mathrm{Re}[\Sigma_\lambda(\boldsymbol{k},\omega)]$ of the quasiparticle self-energy can be calculated, at least in principle, from the Kramers-Kronig transform of $\mathrm{Im}[\Sigma_\lambda(\boldsymbol{k},\omega)]$. A more convenient way to handle the numerical evaluation of $\mathrm{Re}[\Sigma_\lambda(\boldsymbol{k},\omega)]$ is to employ the Quinn-Ferrell line-residue decomposition [29].

Our main results for the quasiparticle spectral function $\mathcal{A}(\boldsymbol{k},\omega)$ are summarized in Figs. 1 and 3. Notably, the presence of the hBN substrate is responsible for the appearance of a family of sharp dispersive satellite features associated with the PP modes and plasmon modes. This is particularly clear in the one-dimensional cut at $\boldsymbol{k} = 0$ of $\mathcal{A}(\boldsymbol{k},\omega)$ displayed in Fig. 3(a) for $d = 10$ nm. All the sharp features between the quasiparticle peak slightly below $\hbar\omega = -0.4$ eV and the peak at $\hbar\omega \approx -0.7$ eV, which is mostly plasmonic in nature, are sensitive to the detailed distribution and dispersion of PP modes in the hBN slab. The latter are tunable by varying the slab thickness d. As illustrated in Figs. 3(b) and 3(c), these peaks shift by several meV when d is changed from 10 nm to 60 nm with ε_F kept constant.

In summary, the coupling between Fabry-Perót phonon-polariton modes in a hyperbolic crystal slab and plasmons in a nearby graphene sheet yields a complex spectrum of hybrid modes. The modes with group velocity equal to the graphene Fermi velocity couple strongly to graphene quasiparticles, enabling direct ARPES access to these modes. Our calculations indicate that the mode frequencies can be easily tuned by varying the slab thickness, as illustrated in Figs. 1 and 3. We note that plasmon-related satellite spectral features tend to be quite robust in the presence of disorder [27], as demonstrated experimentally in Ref. [23]. We also note that the large-area graphene and hBN stacks, which were grown recently by chemical vapor deposition and characterized by ARPES [30], can provide a natural setting for testing the predictions of our work.

We gratefully acknowledge F. H. L. Koppens for useful discussions. This work was supported by the EC under the Graphene Flagship program (Contract No. CNECT-ICT-604391) (A. T. and M. P.), MIUR (A. T. and M. P.) through the programs "FIRB—Futuro in Ricerca 2010"—Project "PLASMOGRAPH" (Grant No. RBFR10M5BT) and "Progetti Premiali 2012"—Project "ABNANOTECH," the U.S. Department of Energy under Grant No. DE-FG02-05ER46203 (A. P.), and a Research Board Grant at the University of Missouri (A. P.). Work at MIT was supported as part of the Center for Excitonics, an Energy Frontier Research Center funded by the U.S. Department of Energy, Office of Science, Basic Energy Sciences under Award No. desc0001088. This work was also supported, in part, by the U.S. Army Research Laboratory and the U.S. Army Research Office through the Institute for Soldier Nanotechnologies, under Contract No. W911NF-13-D-0001. Free software [31] was used.

*levitov@mit.edu
†marco.polini@icloud.com

[1] A. Poddubny, I. Iorsh, P. Belov, and Y. Kivshar, Nat. Photonics **7**, 948 (2013).
[2] S. Dai, Z. Fei, Q. Ma, A. S. Rodin, M. Wagner, A. S. McLeod, M. K. Liu, W. Gannett, W. Regan, K. Watanabe, T. Taniguchi, M. Thiemens, G. Dominguez, A. H. Castro Neto, A. Zettl, F. Keilmann, P. Jarillo-Herrero, M. M. Fogler, and D. N. Basov, Science **343**, 1125 (2014).
[3] J. D. Caldwell, A. Kretinin, Y. Chen, V. Giannini, M. M. Fogler, Y. Francescato, C. T. Ellis, J. G. Tischler, C. R. Woods, A. J. Giles, M. Hong, K. Watanabe, T. Taniguchi, S. A. Maier, and K. S. Novoselov, Nat. Commun. **5**, 5221 (2014).
[4] T. Byrnes, N. Y. Kim, and Y. Yamamoto, Nat. Phys. **10**, 803 (2014).
[5] P. Li, M. Lewin, A. V. Kretinin, J. D. Caldwell, K. S. Novoselov, T. Taniguchi, K. Watanabe, F. Gaussmann, and T. Taubner, arXiv:1502.04093.
[6] S. Dai, Q. Ma, T. Andersen, A. S. McLeod, Z. Fei, M. K. Liu, M. Wagner, K. Watanabe, T. Taniguchi, M. Thiemens, F. Keilmann, P. Jarillo-Herrero, M. M. Fogler, and D. N. Basov, Nat. Commun. **6**, 6963 (2015).
[7] A. Damascelli, Z. Hussain, and Z.-X. Shen, Rev. Mod. Phys. **75**, 473 (2003).
[8] B. Amorim, J. Schiefele, F. Sols, and F. Guinea, Phys. Rev. B **86**, 125448 (2012).
[9] V. W. Brar, M. S. Jang, M. Sherrott, S. Kim, J. J. Lopez, L. B. Kim, M. Choi, and H. Atwater, Nano Lett. **14**, 3876 (2014).
[10] A. Principi, M. Carrega, M. B. Lundeberg, A. Woessner, F. H. L. Koppens, G. Vignale, and M. Polini, Phys. Rev. B **90**, 165408 (2014).
[11] A. Woessner, M. B. Lundeberg, Y. Gao, A. Principi, P. Alonso-González, M. Carrega, K. Watanabe, T. Taniguchi, G. Vignale, M. Polini, J. Hone, R. Hillenbrand, and F. H. L. Koppens, Nat. Mater. **14**, 421 (2015).
[12] S. Dai, Q. Ma, S.-E. Zhu, M. K. Liu, T. Andersen, Z. Fei, M. Goldflam, M. Wagner, K. Watanabe, T. Taniguchi, M. Thiemens, F. Keilmann, G. C. A. M. Janssen, P. Jarillo-Herrero, M. M. Fogler, and D. N. Basov, Nat. Nanotechnol. **10**, 682 (2015).
[13] A. Kumar, T. Low, K. H. Fung, P. Avouris, and N. X. Fang, arXiv:1502.04672.
[14] For reviews on graphene plasmons see, e.g., A. N. Grigorenko, M. Polini, and K. S. Novoselov, Nat. Photonics **6**, 749 (2012); T. Low and P. Avouris, ACS Nano **8**, 1086 (2014).
[15] See Supplemental Material at http://link.aps.org/supplemental/10.1103/PhysRevLett.115.087401, which includes Refs. [16,17], where we present analytical details on the phonon-polariton dispersion and further numerical results on the quasiparticle decay rates and spectral function.
[16] L. D. Landau and E. M. Lifshitz, *Course of Theoretical Physics: Electrodynamics of Continuos Media* (Pergamon, New York, 1984).
[17] L. V. Keldysh, Pis'ma Zh. Eksp. Teor. Fiz. **29**, 716 (1979).
[18] R. Geick, C. H. Perry, and G. Rupprecht, Phys. Rev. **146**, 543 (1966).
[19] G. F. Giuliani and G. Vignale, *Quantum Theory of the Electron Liquid* (Cambridge University Press, Cambridge, England, 2005).
[20] B. Wunsch, T. Stauber, F. Sols, and F. Guinea, New J. Phys. **8**, 318 (2006); E. H. Hwang and S. Das Sarma, Phys. Rev. B **75**, 205418 (2007); A. Principi, M. Polini, and G. Vignale, Phys. Rev. B **80**, 075418 (2009).
[21] A. Bostwick, T. Ohta, T. Seyller, K. Horn, and E. Rotenberg, Nat. Phys. **3**, 36 (2007).
[22] S. Y. Zhou, G.-H. Gweon, A. V. Fedorov, P. N. First, W. A. der Heer, D.-H. Lee, F. Guinea, A. H. Castro Neto, and A. Lanzara, Nat. Mater. **6**, 770 (2007).
[23] A. Bostwick, F. Speck, T. Seyller, K. Horn, M. Polini, R. Asgari, A. H. MacDonald, and E. Rotenberg, Science **328**, 999 (2010).
[24] A. L. Walter, A. Bostwick, K.-J. Jeon, F. Speck, M. Ostler, T. Seyller, L. Moreschini, Y. J. Chang, M. Polini, R. Asgari, A. H. MacDonald, K. Horn, and E. Rotenberg, Phys. Rev. B **84**, 085410 (2011).
[25] D. A. Siegel, C.-H. Park, C. Hwang, J. Deslippe, A. V. Fedorov, S. G. Louie, and A. Lanzara, Proc. Natl. Acad. Sci. U.S.A. **108**, 11365 (2011).
[26] M. Polini, R. Asgari, G. Borghi, Y. Barlas, T. Pereg-Barnea, and A. H. MacDonald, Phys. Rev. B **77**, 081411(R) (2008).
[27] E. H. Hwang and S. Das Sarma, Phys. Rev. B **77**, 081412(R) (2008).
[28] B. I. Lundqvist, Phys. Kondens. Mater. **6**, 193 (1967); **6**, 206 (1967); **7**, 117 (1968); L. Hedin, B. I. Lundqvist, and S. Lundqvist, Solid State Commun. **5**, 237 (1967). It has been claimed [J. Lischner, D. Vigil-Fowler, and S. G. Louie, Phys. Rev. Lett. **110**, 146801 (2013)] that these additional solutions of the Dyson equation disappear when one goes beyond RPA. However, it has been shown that the decay rate and the spectral function still display peaks associated with the collective modes of the electron liquid.
[29] J. J. Quinn and R. A. Ferrell, Phys. Rev. **112**, 812 (1958).
[30] S. Roth, F. Matsui, T. Greber, and J. Osterwalder, Nano Lett. **13**, 2668 (2013).
[31] www.gnu.org; www.python.org.